



HAL
open science

Formaldehyde (HCHO) in air, snow and interstitial air at Concordia (East Antarctic plateau) in summer

S. Preunkert, Michel Legrand, M. Frey, Alexandre Kukui, Joël E Savarino, H.
Gallée, M. King, Benjamin Jourdain, W. Vicars, D. Helmig

► **To cite this version:**

S. Preunkert, Michel Legrand, M. Frey, Alexandre Kukui, Joël E Savarino, et al.. Formaldehyde (HCHO) in air, snow and interstitial air at Concordia (East Antarctic plateau) in summer. *Atmospheric Chemistry and Physics Discussions*, 2014, 14 (23), pp.32027-32070. 10.5194/acpd-14-32027-2014 . hal-01164674v1

HAL Id: hal-01164674

<https://insu.hal.science/hal-01164674v1>

Submitted on 13 Apr 2015 (v1), last revised 17 Jun 2015 (v2)

HAL is a multi-disciplinary open access archive for the deposit and dissemination of scientific research documents, whether they are published or not. The documents may come from teaching and research institutions in France or abroad, or from public or private research centers.

L'archive ouverte pluridisciplinaire **HAL**, est destinée au dépôt et à la diffusion de documents scientifiques de niveau recherche, publiés ou non, émanant des établissements d'enseignement et de recherche français ou étrangers, des laboratoires publics ou privés.

Abstract

During the 2011/12 and 2012/13 austral summers HCHO was investigated for the first time in ambient air, snow, and interstitial air at the Concordia site located near Dome C on the East Antarctic plateau by deploying an Aerolaser AL-4021 analyser. Snow emission fluxes were estimated from vertical gradients of mixing ratios observed between 1 cm and 1 m above the snow surface as well as between interstitial air a few cm below the surface and in air just above the snow-pack. Typical flux values range between 1 to 2×10^{12} molecules $\text{m}^{-2} \text{s}^{-1}$ at night and 3 to 5×10^{12} molecules $\text{m}^{-2} \text{s}^{-1}$ at noon. Shading experiments suggest that the photochemical HCHO production in the snowpack at Concordia remains negligible compared to temperature-driven air–snow exchanges. At 1 m above the snow surface, the observed mean mixing ratio of 130 pptv and its diurnal cycle characterized by a slight decrease around noon are quite well reproduced by 1-D simulations that include snow emissions and gas phase methane oxidation chemistry.

1 Introduction

HCHO represents an important source of RO_2 radicals in the remote atmosphere of Antarctica, and is therefore intimately linked to the oxidative capacity of the atmosphere in these regions. This is true in margin regions of Antarctica as concluded on the basis of examinations of the observed HO_x budgets at Halley (Bloss et al., 2007) and Dumont d'Urville (DDU, Kukui et al., 2012). At these two coastal sites, the HCHO budget was recently discussed by Preunkert et al. (2013), who concluded that, depending on the oxidative character of the local atmosphere and on the thickness and stability of the atmospheric boundary layer, either the methane oxidation by OH followed by reaction with NO, or snow emissions from neighbouring snow covered regions dominate the HCHO budget. At DDU the largest HCHO source is the methane oxidation in relation with a level of oxidants 3 times higher compared to Halley, and more frequent air mass

32029

transport from inland Antarctica there. At Halley, the shallower boundary layer makes snow emissions the dominant HCHO source.

The examination of the observed HO_x budget at the South Pole (Chen et al., 2004) and Concordia (Kukui et al., 2014) pointed out the role of HCHO on the RO_2 budget over the Antarctic plateau. At the South Pole, Hutterli et al. (2004) quantified snow-air fluxes on the basis of both atmospheric vertical gradients and firn air measurements. It has to be emphasized that the South Pole remains up to now the single Antarctic site where such a direct quantification of snow HCHO emissions was done.

The aims of the present study are (1) to document the boundary layer HCHO mixing ratio at Concordia during the OPALE (Oxidant Production over Antarctic Land and its Export) project (Preunkert et al., 2012) (see also Kukui et al., 2014), (2) to quantify the summer HCHO snow emissions under conditions encountered at day and night at Concordia, and (3) to compare the role of snow emissions with that of the gas-phase production of HCHO in central Antarctica.

2 Methods and field campaigns

2.1 HCHO measurements

HCHO measurements were performed using a commercial Aerolaser analyzer (AL-4021). The technique, a continuous liquid fluorimetry, has been described in detail elsewhere (Dasgupta et al., 1988). Gaseous HCHO is scrubbed into a diluted sulfuric acid solution followed by reaction with the Hantzsch reagent, a dilute mixture of acetyl acetone, acetic acid, and ammonium acetate. Aqueous-phase formaldehyde reacts with the Hantzsch reagent to produce a fluorescent compound that is detected at 510 nm. The working conditions applied to the AL 4021 deployed at Concordia were similar to those applied by Preunkert et al. (2013) in their study conducted at the coastal Antarctic site of Dumont D'Urville. In brief, raw data are monitored with a time resolution of 30 s, gas standard calibration and zero determinations are made every 12 and

32030

2 h, respectively. While Preunkert et al. (2013) used an air flow of 2 L STP min^{-1} (leading to a stripping efficiency of 98 %) in view to obtain accurate HCHO measurements of the low winter levels encountered at DDU, the flow rate was set here when possible (see Sect. 2.3) to 1 L STP min^{-1} , as recommended by Aerolaser company, to reach a stripping efficiency of more than 99 % (M. Haaks, personal communication 2011). As discussed by Preunkert et al. (2013), to minimize effects of changing temperatures in the laboratory at Concordia, the monitor was run in a box that was thermostated at 20°C .

2.2 The 2011/12 field experiments

The second OPALE field campaign took place at Concordia located over the high East Antarctic plateau ($75^\circ 06' \text{ S}$, $123^\circ 33' \text{ E}$) from late November 2011 to mid-January 2012. Atmospheric HCHO was measured at 1 m (Fig. 1a) and 1 cm (not shown) above the snow surface at a place located $\sim 900 \text{ m}$ south-southwest from the main station. Two 15 m long PTFE tubes (4 mm internal diameter) were used to bring ambient air sampled at the two heights into the field laboratory. Through the tubes, air was sucked with an external pump at a flow rate of 4 to 6 L min^{-1} to keep its residence time in the lines low enough to maintain potential losses below 5 % (see details in Preunkert et al., 2013). To avoid condensation, the airlines were heated. In turn of 15 min the air inlet of the AL-4021 is connected to these tubes via a 50 cm long PTFE tube (internal diameter 4 mm) and a PTFE coated 3-way electro valve. The tightness of the sampling line was regularly controlled. Comparison of the two 15 m long airlines made by putting their air entries at the same height (1 m) showed no systematic differences (mean difference of 2.5 pptv over 10 h).

The detection limit of the analyzer calculated as twice the SD of raw data (30 s) obtained during the 25 min zero measurements, which were made every 2 h, is reported in Fig. 1b. Over the first two weeks of the sampling period, the detection limit remained low and similar to what was observed with the same analyzer ($\sim 30 \text{ pptv}$) during the

32031

year-round study conducted at DDU by Preunkert et al. (2013). During the second half of the sampling period at Concordia, the detection limit was enhanced exceeding 100 pptv on 30 December, due to a recurrent presence of air bubbles in the analyzer.

HCHO measurements started on 14 December but were interrupted several times after 3 January due to problems with the fluorimeter of the AL-4021 (see Fig. 1 for data availability). During the sampling period, no significant snowfall event took place and the main wind direction was from the southeast to southwest. However, several episodes (spanning 18 % of the total time) with wind blowing from North (from 30° W to 60° E sector, i.e. the direction of the station) were encountered (Fig. 1c). Two major North wind periods took place from 30 December to 1 January in the morning and most of time after 9 January (Fig. 1c). Over these events, scattered HCHO values were often observed and removed from the data set (see red points in Fig. 1a).

Due to either the presence of air bubbles in the analyzer, leading to a detection limit well above 30 pptv, or to scattered values related to contamination from station activities, qualified data on atmospheric HCHO at 1 cm and 1 m above the snow surface (see Sect. 4) are limited to the period of 14 to 29 December. Anyway, note that the HCHO mixing ratio at 1 m ($131 \pm 45 \text{ pptv}$ calculated with the few data available between 1 and 11 January, see the horizontal dashed line in Fig. 1a) remains similar to the mean value of $127 \pm 31 \text{ pptv}$ observed between 14 and 28 December.

Concurrent atmospheric measurements, which are relevant for discussion, include NO , OH , RO_2 , and methylhydroperoxide (MHP). NO was determined with a 2-channel chemiluminescence detector following working conditions detailed in Frey et al. (2013) and Frey et al. (2014). The OH and RO_2 radicals were measured using chemical ionisation mass spectrometry (Kukui et al., 2012; Kukui et al., 2014). During the campaign the photolysis rates of HCHO were documented using a 2π spectroradiometer (Metcon company). MHP was measured together with H_2O_2 deploying an Aerolaser AL-2021 instrument as during the first OPALE campaign conducted at DDU (Preunkert et al., 2012).

32032

Sciences) previously passivized with O₃ were placed at all ST inlets to protect them from ice crystals.

During the campaign, sampled air was provided to the AL-4021 and to each of the other running analyzers (NO_x, Hg, and CO, not discussed here), with a flow rate of 1 L min⁻¹ (i.e. 0.7 L STP min⁻¹). Therefore, the airflow of the AL-4021 was set to 0.6 L STP min⁻¹ what is 40 % lower than the one normally applied for the AL-4021 (see Sect. 2.1), resulting in an ~ 25 % lower sensibility of the instrument. Taken as twice the SD of zero measurements, the detection limit was 67 ± 22 pptv from 22 December to 6 January (151 zero measurements) and 120 ± 55 pptv from 6 to 25 January (185 zero measurements). Compared to other experiments performed with the device (see Sect. 2.2) these rather high detection limits were generated by frequent arrivals of air bubbles in the analyzer. Twice per week, the inlets of the 3 MT lines were placed for 1 h at 2 m height, showing no systematic differences (4 ± 21 and 5 ± 29 pptv with respect to one inlet reference). Such a comparison of the different airlines was not possible for ST2 since HCHO measurements started well after their set up in snow.

As seen in Fig. 2a, overall means of HCHO air mixing ratios measured at MT through the 11, 2 and 0.3 m inlets are 164 ± 55, 168 ± 54 and 170 ± 61 pptv, respectively. The mean value observed at 20 cm above the snow surface at ST2 is 203 ± 55 pptv. From 20 to 22 December, HCHO was sampled at 20 cm above the surface by using a 3 m long PTFE line (internal diameter 4 mm) connected directly to the AL-4021, giving a mixing ratio of 135 ± 48 pptv. In view of the high variability encountered for HCHO measurements during this experiment, these values show no significant difference. However, the relative high mean atmospheric HCHO mixing ratios measured at ST2 might be also related to the fact that ST air lines were not flushed continuously but only for 10 min each 2 h. Thus, absolute atmospheric HCHO mixing ratios are not investigated with this 2012/13 data set, but the measurements will be used to examine HCHO in interstitial air (see Sect. 4.2), in view to derive HCHO fluxes between the snow pack and the atmosphere (Sect. 5.2) and to discuss its firn-air equilibrium (Sect. 5.3).

32035

2.4 Model calculations

Observed HCHO mixing ratios (daily mean and diurnal variation) were compared with those simulated by a 1-D box model that considers snow HCHO emissions as well as the local gas-phase photochemistry. For snow emissions, we used values derived from the observed vertical gradient between 1 cm and 1 m above the snow surface as well as those derived from the observed difference between snow interstitial air and air above the snow surface (see Sect. 5). For calculations of the gas phase photochemistry we considered the model used by Preunkert et al. (2013) to examine the budget of HCHO at the Antarctic coast that includes the CH₄ oxidation as well as the oxidation of non-methane hydrocarbons (light alkenes and DMS) together with major sinks of HCHO (its photolysis and reaction with OH). For simulations at Concordia, we neglected the oxidation of ethene and DMS oxidation pathways. Indeed, even with a DMS summer mixing ratio of 50 pptv at DDU (against less than 1 pptv at Concordia, Preunkert et al., 2008), and an ethene level of 17 pptv (against less than 3 pptv expected for Concordia as measured at South Pole, Beyersdorf et al., 2010), Preunkert et al. (2013) concluded that the gas phase production of HCHO from DMS and non-methane hydrocarbons only represents a few percent of the gas phase production (i.e. ~ 4 %) dominated by the methane oxidation. The 15 gas-phase reactions considered in this work (see Table 1) will also permit to evaluate the influence of the bromine chemistry.

The vertical transport of the 1-D model was represented using vertical distribution of turbulent diffusion coefficients (K_z) calculated by the regional atmospheric MAR model (Modèle Atmosphérique Régional). More details of MAR and of its reliability at Concordia during the OPALÉ campaign are given in Gallée and Gorodetskaya (2008) and Gallée et al. (2014). Similarly to calculations performed by Legrand et al. (2014), we used the MAR data obtained with a horizontal resolution of 20 km centered at Concordia, a vertical resolution of 0.9 m for the height of up to 23 m above the surface decreasing upward to about 50 m at the height of 500 m and to ~ 1800 m at the top level of ~ 24 km. For the 1-D model, the K_z values were linearly interpolated to the

32036

4 HCHO in the snowpack

4.1 HCHO in snow

Figure 4a shows the bulk snow HCHO profiles obtained in the two snow-pits dug at Concordia during the 2011/12 campaign (Sect. 2.2). The good agreement of data between the snow-pit dug 27 December near the air sampling site and the 9 January one dug at 3 km from the station suggests that station activities had little impact on the HCHO content of the snowpack in the immediate vicinity of the station. Note that the two profiles are also in good agreement with the one made by Hutterli et al. (2002) in January 1998 (i.e. well before the start in 2003 of overwintering station activities at Concordia).

The three depth profiles show a similar decreasing trend with depth reaching a value of 0.2–0.3 ppbw below 70 cm depth. Some differences exist between the three profiles with a maximum of 1 ppbw measured by Hutterli et al. (2002) at the surface against lower values in this study. Indeed, with individual values ranging from 0.2 to 0.4 ppbw, the 26 skin layer snow samples (Sect. 2.2) show mean levels (0.27 ± 0.05 ppbw from 26 to 27 December and 0.29 ± 0.07 ppbw from 2 to 4 January) that are well below the maximum seen in the snow-pit profiles (0.8 ppbw at 8 cm depth for the 27 December pit and 1.0–1.2 ppbw between 5 and 15 cm depth in the 9 January pit). Such a large variability in the HCHO mixing ratios in the uppermost snow layers was often reported in previous studies conducted at other polar sites. It has been suggested that this is due to the presence or absence of freshly deposited snow that is always more enriched in HCHO with respect to atmospheric mixing ratios than aged snow layers (Hutterli et al., 1999, 2002, and 2004). Under Concordia conditions, as discussed in Sect. 4.3, snow in equilibrium with the atmosphere in summer would contain at least 2.6 ppbw of HCHO.

In the 9 January snow-pit, the maximum of HCHO mixing ratios seen from 5 to 15 cm below the surface (Fig. 4b) coincides with two relative maxima of sodium suggesting that they correspond to winter snow layers. Given the typical snow accumulation of 10 cm of snow at Concordia these two depths correspond to winter 2011 and winter

32039

2010. For the 27 December snow-pit, the wide maximum of HCHO still coincides with these two winter layers seen in the corresponding sodium profile. The HCHO profile obtained by Hutterli et al. (2002) is more flat with a less variable value between 5 and 25 cm below the surface. In the absence of sodium data in this previous study, it remains difficult to conclude whether that is due to a strong wind driven redistribution of summer and winter snow layers by the wind at the snow pit location sampled by Hutterli et al. (2002) in 1999.

HCHO snow-pit profiles are also available from South Pole (Hutterli et al., 2004) and Summit in central Greenland (Hutterli et al., 1999). At both sites, winter HCHO maxima close to ~ 4 –6 ppbw were observed. Deeper in the snow at 1.6 m depth, concentrations decrease to a nearly constant level of 4 ppbw at Summit and 0.3–1.1 ppbw at South Pole. The higher concentration observed in deeper snow layers at Summit than at South Pole was suggested to be driven by the fact that the mean snow accumulation rate is higher at Summit ($22 \text{ g H}_2\text{O cm}^{-2} \text{ yr}^{-1}$) than at South Pole (6 – $11 \text{ g H}_2\text{O cm}^{-2} \text{ yr}^{-1}$) (Hutterli et al., 2002). The larger snow accumulation at Summit permits a better preservation of the atmospheric signal that dominates the weaker uptake capacity of HCHO in snow and ice at warmer temperatures (Burkhart et al., 2002; Barret et al., 2011a) at Summit compared to South Pole (mean annual T of -31°C instead of -49°C at South Pole). Thus, considering the quite similar temperatures at Concordia and South Pole (mean annual T of -54°C compared to -49°C at South Pole), the lower mean snow accumulation ($2.8 \text{ g H}_2\text{O cm}^{-2} \text{ yr}^{-1}$ compared to 6 – $11 \text{ g H}_2\text{O cm}^{-2} \text{ yr}^{-1}$ at South Pole) may reduce the preservation there, explaining the lower content in deep snow layers at Concordia than at South Pole.

4.2 HCHO in interstitial Air

During both the 2011/12 and 2012/13 field campaigns, investigations were made to document HCHO in the interstitial firn air (Fig. 5). The mean value observed at 20 cm depth in 2012/13 (530 ± 95 pptv) largely exceeds the one in the atmosphere (~ 130 pptv observed in 2011/12 and 135–170 pptv observed in 2012/13). Similar enhancements of

32040

HCHO in firn air have been seen in a previous study conducted at South Pole (750 pptv at 10 cm depth against 103 pptv in the atmosphere, Hutterli et al., 2004). Figures 4 and 5 show that, similar to the HCHO profile in snow, firn air HCHO levels show highest values near the snow surface and decreasing levels with depth, reaching values lower than 100 pptv below 80 cm depth. Whereas the here presented data of the HCHO change with depth in firn air is unique for Antarctica (no depth profile of interstitial air content is available from South Pole) a similar depth profile has been reported for Summit by Hutterli et al. (1999), with 1500–2000 pptv at 5–20 cm below the snow surface (compared to 230 pptv in the atmosphere) and 400 pptv at 1.5 m below the surface. The elevated mixing ratios in the firn air at Concordia with respect to those in the atmosphere point out the snowpack as a source of HCHO for the atmosphere in summer.

As seen in Fig. 6, HCHO mixing ratios measured at –20 cm in firn air coincide more closely with the daily course of temperature measured above the surface and at –20 cm than with the daily course of irradiance peaking at noon. Thus, the temperature variation in the uppermost snow layers should drive the HCHO firn air mixing ratios there, which tend to increase at warmer temperatures. In addition, during the first week of January the daily mean HCHO mixing ratio at –20 cm (600 pptv) was higher than the one after 9 January (400 pptv) in relation with a decrease of the temperature from –27.5 to –31.3 °C. This dependence of HCHO firn air in the upper snow-pack will be discussed further in the next section.

4.3 The firn air–snow partitioning at Concordia

4.3.1 The HCHO-ice thermodynamic equilibrium

On the basis of laboratory experiments, two studies investigated the HCHO partitioning between air and ice. The first attempt was made by Burkhart et al. (2002) who conducted laboratory experiments with pure ice between –5 and –35 °C. However, as emphasized by Burkhart et al. (2002), the duration of laboratory experiments (less

32041

than 2 days) was not long enough to permit the ice to reach equilibrium, in particular at –35 °C. In a more recent study Barret et al. (2011a) measured the solubility and the diffusivity of HCHO in ice between –7 and –30 °C showing that the partitioning of HCHO between snow and atmosphere can be described by $K(T) = X_{\text{HCHO}} / (P_{\text{HCHO}})^{0.803}$ (with X_{HCHO} being the HCHO molar fraction, P_{HCHO} being in Pa and T in K), in which $K(T)$ follows an Arrhenius law. This equilibrium law is reported in Fig. 7 (black solid line) along with the one (black dashed line) from Burkhart et al. (2002), the large difference between the two derived laws at low temperatures clearly reveals the under-saturation of the ice in the experiments conducted by Burkhart et al. (2002).

A few studies attempted to compare the partitioning of HCHO between air and snow observed during field campaigns with the thermodynamic equilibrium obtained in laboratory studies. This was done by Burkhart et al. (2002) with bulk snow and firn air data obtained by Hutterli et al. (1999) in a 3 m snow-pit dug at Summit. Barret et al. (2011b) examined whether the Alaskan Arctic snowpack follows the thermodynamic equilibrium. However, it has to be emphasized that in this later study, air concentrations were not measured in the snowpack and were assumed to be identical to those measured 60 cm above the surface snow (see discussions below). Even more limited were examinations of the HCHO partitioning between air and snow in Antarctica as firn air measurements are very rarely available there. Hutterli et al. (2004) performed a few firn air measurements at 10 cm below the surface at South Pole in December 2000. These previous data (Summit, Barrow, and South Pole) are reported in Fig. 7 together with those gained in this study at Concordia. Due to the existence of a residual diurnal temperature cycle at 20 cm below the surface (see Fig. 6), data from this depth were reported in Fig. 7 as 10 min means, while those from further down were averaged over each of the 6 periods assigned in Fig. 2. The X_{HCHO} values used in calculations of $K(T)$ reported in Fig. 7 were derived from the mean snow-pit profile reported in Fig. 4.

As seen in Fig. 7, all data from Concordia indicate under-saturation of snow by a factor of 10 with respect to interstitial air. We notice that, whereas no significant difference appears between the two sets of data derived using firn air values collected in 2011/12

and 2012/13, data corresponding to -70 cm in the 2012/13 experiment show systematically lower $K(T)$ values. This latter difference is caused by the relatively high firn air mixing ratios seen at 70 cm depth in 2012/13 when compared to observations made just above and below (see Fig. 5). Thus we can not exclude that the firn air sampling at this depth might have been somewhat over-estimated as it might happen due to the presence of an inhomogeneous structure of the snow pack (i.e. depth hoar and/or wind crusts) what might have brought air from above to the inlet.

At the first glance, Fig. 7 suggests that the strong under-saturation of snow at Concordia is very unique compared to the other sites. However, as already mentioned, the Barrow data that considered atmospheric (and not firn air) mixing ratios certainly have led to a significant underestimation of the degree of under-saturation of snow. Furthermore, the single point reported for South Pole in Fig. 7 is calculated with 3.2 ppbw of bulk snow HCHO and a firn air value of 750 pptv (Hutterli et al., 2004), which is however probably diluted by atmospheric air (Hutterli et al., 2004) leading to an underestimation of the degree of under-saturation of snow. Finally, at Summit, where snow and firn air profiles are well documented down to 2.5 m depth, a super-saturation was found at the surface followed by striking under-saturation 5 cm below the surface. Further down, at the depth of the preceding winter, an almost perfect thermodynamic equilibrium was observed. Then, except in the layer corresponding to the previous summer where snow is again under-saturated, most of the snow down to 2.5 m was close to the equilibrium. In conclusion, apart from Summit (with the noticeable exception of the snow located just below the surface), the polar snow appears often under-saturated with a particularly large depletion at Concordia. Note that, since a net HCHO flux out of the snow is detected during day and night at Concordia, the here calculated under saturation needs to be considered even as an upper value.

It is out of the scope of the present paper to investigate in detail the observed under-saturation of snow. At this stage we only assume (similarly as Hutterli et al., 1999) that there is a process acting in summer, leading to a strong under saturation of firn with respect to the thermodynamic air–ice equilibrium. This under saturation is counteracted

32043

by (1) precipitation, fog and frost events which add super saturated snow to the existing snowpack (Hutterli et al., 2004; Jacobi et al., 2001; Barret et al., 2011b), and (2) HCHO rich snow layers further down originating from the preceding winter season (Hutterli et al., 1999, 2003). If the snow accumulation is, however extremely low as at in Dome C, the preceding winter layer is still near the surface in summer, and super saturated fresh snow is added only seldomly to the snowpack. As a result, the regime of extreme under saturation acts probably throughout the entire snowpack, confirmed by our measurements, at least in snow layers down to 1 m corresponding to ages of the last ~ 10 year. However designing a more sophisticated modeling approach would require further data from Concordia obtained during winter in view to gain year-round information of HCHO in atmospheric air as well as in the interstitial air in the upper centimeters of the snow-pack

As already shown by Fig. 6, Fig. 7 suggests a temperature driven dependence of the firn air–snow partitioning at Concordia. The slope of the linear regression obtained with data at -20 cm in the Arrhenius law in Fig. 7 ($R^2 = 0.5$), for which a large range of temperature is encountered, is quite similar (i.e. only 20% higher) than the one of the thermodynamic equilibrium calculated by Barret et al. (2011a).

4.3.2 Possible photochemical HCHO production in the snow-pack

As discussed in the preceding section, the assumption that snow emissions are controlled by temperature-driven exchanges (Hutterli et al., 2003) seems to be confirmed for Concordia conditions. While different experiments conducted at Alert and Barrow (Canadian and Alaskan Arctic) showed that HCHO emissions due to photolytic degradation of organic matter are present there (Barret et al., 2011b and references therein), this photolytic HCHO production seems to be very limited at inland polar ice sheet sites such as Summit (Hutterli et al., 1999) and South Pole (e.g. $< 20\%$ at South Pole) (Hutterli et al., 2004). To check directly whether the conclusion drawn for South Pole remains correct for Concordia, shading experiments were performed in January 2012 (see Sect. 2.2). No impact of cutting incident UV-radiation (wavelengths < 380 nm) on

32044

5.2 Estimations derived from interstitial firn air measurements

In view of the limited time period of available measurements and of the high uncertainty of the HCHO snow flux values derived from the relatively weak vertical HCHO gradients between 1 cm and 1 m (see Sect. 5.1) we try to estimate HCHO snow fluxes also on the base of HCHO gradients observed between the interstitial air and the atmosphere. One advantage of this approach lies in the fact that the transport of HCHO in firn air is slower than the one in the free atmosphere leading to firn-atmosphere gradients that would largely exceed the detection limit of HCHO measurements.

In order to estimate firn air-atmosphere snow fluxes, Fick's Law can be applied using measured concentration gradients between firn air and the atmosphere and the effective diffusion coefficient (D_{eff}) in the open pore space. Since the turbulent diffusion in air above the snow is much larger than the diffusivity in firn air, the main concentration gradient will be in firn. Since HCHO air measurements made in 2011/12 (see Fig. 3) indicate a vertical gradient of only a few pptv it is legitimated to use mixing ratios on the MT inlet at ~ 2 m as representative of HCHO level just above the surface.

Vertical transport in firn air of the top centimeters of the snowpack will depend on the molecular diffusion but can be significantly increased at high wind speed due to forced ventilation (Albert, 2002). Following Schwander et al. (1989) an effective molecular diffusion in firn (D_{eff}) close to $1.3 \times 10^{-5} \text{ m}^2 \text{ s}^{-1}$ is calculated for conditions at Concordia (at 650 mbar, 244 K and a snow density of 0.35 g cm^{-3}). Previous studies dealing with firn air-atmosphere gradients in Antarctica (Hutterli et al., 2004; Frey et al., 2005) assumed that with wind speed lower than 5 m s^{-1} , the wind pumping should have no significant influence with respect to molecular diffusion on motion in firn. However, more recently Seok et al. (2009) found a anti-correlation between wind speed and CO_2 firn air gradients in the winter snowpack at a subalpine site in Colorado even at low wind speeds (a decrease by 50 % of the gradient when wind speed increases from 0 to 3 m s^{-1}). Therefore, we examine the dependence of the HCHO gradients between -20 cm and the atmosphere at Concordia with air temperature and wind speed data. The multi re-

32047

gression of HCHO gradients ($R^2 = 0.5$) suggests a ~ 50 pptv decrease of the HCHO gradient when the wind speed reaches 5 m s^{-1} , what can make up to $\sim 10\%$ of HCHO gradients during certain time periods. Therefore, this effect of forced ventilation was considered in the HCHO flux reported below.

The approach used here to estimate the fluxes assumes a constant diffusivity coefficient and thus a linear change of mixing ratios between the two measurement levels. As discussed in Sect. 4, HCHO firn air levels are expected to reach a maximum in the uppermost 10 cm of the snowpack and therefore the use of firn air data at -20 cm would significantly underestimate the calculated HCHO fluxes. Therefore, an attempt was made to estimate HCHO mixing ratios in firn air near the surface by using the overall observed partitioning between snow and firn air observed at -20 cm below the surface (Fig. 7) as a function of temperature, and the mean snow pit content measured between 4 and 10 cm (means of 0.80 and 0.94 ppb). The daily course of the firn temperature at 7 cm below the surface was taken as the mean of air and snow (at 20 cm below the surface) temperatures.

Figure 6 shows results obtained over two periods of the 2012/13 experiment, during which different mean air temperatures were encountered. It can be seen that HCHO levels at -7 cm are clearly enhanced (up to 240 pptv) compared to HCHO levels measured at -20 cm during the day, but are similar to the latter ones at night. Following calculations described above, mean HCHO fluxes out of the snow of $2.6 \pm 0.8 \times 10^{12}$ and $1.8 \pm 0.7 \times 10^{12} \text{ molecule m}^{-2} \text{ s}^{-1}$ are calculated for the two periods during which mean air temperatures of -27.4 and -31.3 °C prevailed, respectively. Note that a significantly lower value ($0.65 \times 10^{12} \text{ molecule m}^{-2} \text{ s}^{-1}$) is calculated for the end of January when mean air temperatures dropped to -37.5 °C.

Applying this approach to the December 2011 campaign over the periods of 14 to 18 December (mean air temperature of -35 °C) and 19 to 28 December (mean air temperature of -29 °C) HCHO fluxes of $0.85 \pm 0.36 \times 10^{12}$ and $2.15 \pm 0.93 \times 10^{12} \text{ molecule m}^{-2} \text{ s}^{-1}$ are estimated, what is (given the uncertainties of ± 3 cm in snow depth and of 0.08 ppbw in bulk snow HCHO) in good agreement with the correspond-

32048

ing flux estimates ($-0.36 \pm 1.6 \times 10^{12}$ molecule $m^{-2}s^{-1}$ from 14 to 18 December and $2.7 \pm 2.7 \times 10^{12}$ molecule $m^{-2}s^{-1}$ from 19 to 28 December) made in Sect. 5.1 on the base of atmospheric vertical gradients.

5 From the bulk snow content and an empirical partitioning between firn and in the snowpack, Hutterli et al. (2002) estimated a summer HCHO snow flux of $\sim 0.2 \times 10^{12}$ molecule $m^{-2}s^{-1}$ at Concordia, thus 10 times lower than is derived from atmospheric and firn air measurements made in our study. Since calculations of Hutterli et al. (2002) are based on a thermodynamic equilibrium, it is very likely that a large part of the difference comes from the large under-saturation of snow with respect to
10 interstitial air as observed at Concordia (Sect. 4.3.1).

6 Sources and sinks of HCHO at Concordia

The importance of local gas phase photochemical productions and snow emissions on the atmospheric HCHO mixing ratios observed at 1 m above the snow surface at Concordia in summer were investigated with 1-D model simulations. We performed
15 calculations only for days with clear sky conditions (see Sect. 2.4). Whereas NO measurements started end of November 2011, those of OH and RO₂ are only available after 19 December and we focus therefore on the period from 19 to 28 December. The model was run each hour to simulate the daily cycle of HCHO mixing ratios. OH, HO₂ (estimated from RO₂ measurements, Kukui et al., 2014), NO, photolytic rates (see
20 Sect. 2.2) and snow emission rates (see Sect. 5) were constrained by measurements. Their mean diurnal cycles are summarized in Fig. 8 together with the one of measured MHP. A CH₄ mixing ratio of 1758 ppbv was used as recorded in December 2011 at the Syowa Antarctic station (69° S). The HCHO snow emission fluxes considered in the model (hereafter denoted net HCHO snow flux) were calculated as the average of
25 F-HCHO values derived from atmospheric HCHO gradients (Sect. 5.1) and of those derived from firn air-atmosphere gradients (Sect. 5.2).

32049

6.1 Gas-phase photochemical sources and sinks of HCHO

In a first step simulations of the gas phase photochemistry only consider the CH₄ oxidation by OH together with the two major sinks of HCHO, namely the photolysis (Reactions R11 and R12, Table 1) and the OH reaction (Reaction R9, Table 1). Hereby
5 the initial OH attack leads to the formation of the methyl peroxy (CH₃O₂) radical which can react with NO to form CH₃O, which is then rapidly converted to HCHO with O₂ (Reactions R1 to R3, Table 1). This reaction sequence is the dominant pathway under high NO conditions as encountered at Concordia whereas at low NO levels it would compete with Reactions (R4) to (R6) (Table 1). Simulations indicate that this methane
10 oxidation pathway leads to steady-state mixing ratios of 56 and 91 pptv at noon and midnight, respectively (Fig. 9a).

MHP can form HCHO, CH₃O or CH₃O₂ (Reactions R7, R8, and R10, Table 1). Since MHP measurements are available, the MHP contribution to the production of HCHO was examined separately from the CH₄ oxidation pathway with OH and NO (Reactions
15 R1 to R6, R9, R11, and R12, Table 1). As seen in Fig. 8, a daily mean MHP mixing ratio of ~ 50 pptv was observed at Concordia, which is nearly one half of the one reported by Frey et al. (2005) for South Pole. On the other hand, our model simulates a MHP mixing ratio of 20 pptv, suggesting that the MHP budget at Concordia is at least to $\sim 40\%$ made up by CH₄ oxidation. Using observed MHP mixing ratios we calculate
20 that ~ 15 pptv of HCHO are linked to the MHP breakdown (Fig. 9). Thus the MHP pathway accounts for 17% of the total HCHO production originating from the CH₄ oxidation at Concordia. That is virtually the same what was obtained at DDU (Preunkert et al., 2013), but only half of the corresponding value (i.e. 36%) observed in the marine boundary layer (Wagner et al., 2002). As already concluded by Preunkert et al. (2013),
25 this is due to the high level of NO, which strengthens the OH/NO methane oxidation pathway (Reaction R2) with respect to the HO₂ and MHP pathway (Reaction R6).

On the basis of DOAS measurements made at Concordia, Frey et al. (2014) estimated that 2 to 3 pptv of BrO are present near the surface. Assuming a daily mean

32050

value of 2.5 pptv of BrO we estimated the Br level to be of 0.43 pptv from steady state calculations considering the BrO photolysis and the Br reaction with O₃. Using these values and considering Reactions (R13)–(R15) of Table 1, we found that the Br chemistry represents a net HCHO loss that remains limited to –3 to –10 pptv from noon to midnight (Fig. 9b).

As seen in Fig. 8a the simulated HCHO daily cycle resulting from the overall gas phase chemistry accounts for 70 and 95 pptv (i.e. 65 and 68 % of the observed HCHO level) at noon and at midnight, respectively. Such a large contribution of the local gas phase chemistry was also found for South Pole, where oxidants are of similar abundance than at Concordia. Thus with 2×10^6 molecules cm⁻³ of OH and 88 pptv of NO (Eisele et al., 2008) consistently to Concordia ~ 70 % of the observed 110 pptv of HCHO were explained by the gas phase chemistry (Hutterli et al., 2004) at South Pole.

6.2 The impact of snow emissions on the HCHO budget

As mentioned in Sect. 3 (see also Fig. 9a) the observed diurnal HCHO cycle in summer is characterized by a daytime minimum with amplitude reaching 45 pptv. The simulated diurnal cycle related to the gas phase chemistry reproduces a similar diurnal cycle but with a slightly weaker amplitude (~ 30 pptv), and simulated HCHO mixing ratios underestimate observations by ~ 40 pptv at noon and ~ 55 pptv at night.

Considering the net HCHO snow flux (see Fig. 8) in addition to the above discussed gas phase chemistry, a daily mean HCHO mixing ratio of 112 pptv is calculated, slightly lower compared to the observed 128 pptv. While simulations are in good agreement from 20:00 to 04:00 LT (Fig. 9a) they tend to underestimate observations by 30 ± 9 pptv from 09:00 to 15:00 LT. The simulated values indicate that HCHO snow emissions account for ~ 30 % of the observed HCHO mixing ratio at night and around 10 % at noon.

Note that, since the values of the HCHO snow emission rates are based on in situ measurements, they represent the net HCHO flux that includes also the effect of dry deposition. Therefore no dry deposition was considered in the simulations.

32051

6.3 Uncertainties of model calculations

Simulations of (gas-phase chemistry plus snow emissions) indicate a better agreement with observations during the night than during the day. We investigated to what extend the uncertainties of simulations depend on the time of day and which parameters are responsible for that. The uncertainties of the preceding calculations include those linked to the kinetic rates of gas phase calculations but are also related to the day to day variability of the hourly values used for OH, HO₂, NO, MHP, photolysis rates and the uncertainty of the net HCHO snow emission flux as reported in Fig. 8. The uncertainty of the simulated turbulent transport needs also to be examined.

To evaluate the uncertainty linked to the kinetic rates of the main gas phase HCHO production processes, a Monte-Carlo study was performed in which all of the rate constants involved in methane oxidation (Reactions R1 to R9, Table 1) were modified simultaneously and independently of each other accordingly to their probability distribution (see Preunkert et al., 2013 and Wagner et al., 2002 for further details). Including 1000 model runs the uncertainty ($\pm 1\sigma$) of calculations related to the kinetic rates is close to ± 10 pptv (i.e. 10 % of calculated values) under daily mean Concordia summer conditions.

A Monte-Carlo study was also applied to evaluate uncertainties resulting from the daily variability of OH, HO₂, NO, MHP, photolysis rates, and the calculated uncertainty of the HCHO net snow emission. The overall HCHO error derived from this Monte-Carlo study reaches ± 13 pptv from 08:00 to 18:00 LT (mean simulated value of 88 pptv) and ± 26 pptv from 20:00 to 04:00 LT (mean simulated value of 140 pptv). Although the 10 % uncertainty of the CH₄ oxidation constant rates are not included in errors reported in Fig. 9a, it can be seen that HCHO simulated values match observations during the night but underestimate them slightly during the day.

Figure 9c indicates the relative contribution of each parameter to the total uncertainty. It can be seen that during the day (from 08:00 to 18:00 LT) the main uncertainty is related to the variability of OH, the uncertainty of the net HCHO snow flux, and the

32052

- Burkhart, J. F., Hutterli, M. A., and Bales, R. C.: Partitioning of formaldehyde between air and ice at -35°C to -5°C , *Atmos. Environ.*, 36, 2157–2163, 2002.
- Chen, G., Davis, D., Crawford, J., Hutterli, L.M., Huey, L.G., Slusher, D., Mauldin, L., Eisele, F., Tanner, D., Dibb, J., Buhr, M., McConnell, J., Lefer, B., Shetter R., Blake D., Song, C.H., Lombardi K., and Arnoldy, J.: A reassessment of HO_x South Pole chemistry based on observations recorded during ISCAT 2000, *Atmos. Environ.*, 38, 5451–5461, doi:10.1016/j.atmosenv.2003.07.018, 2004.
- Dasgupta, P. K., Dong, S., Hwang, H., Yang, H.-C., and Genfa, Z.: Continuous liquid-phase fluorometry coupled to a diffusion scrubber for the real-time determination of atmospheric formaldehyde, hydrogen peroxide and sulfur dioxide, *Atmos. Environ.*, 22, 949–963, doi:10.1016/0004-6981(88)90273-9, 1988.
- DeMore, W. B., Sander, S. P., Golden, D. M., Hampson, R. F., Kurylo, M. J., Howard, C. J., Ravishankara, A. R., Kolb, C. E., and Molina, M. J.: *Chemical Kinetics and Photochemical Data for Use in Stratospheric Modeling*, Evaluation 12, JPL Publ., 97–4, 269 pp., JPL: Pasadena, CA, 15 January 1997.
- Domine, F., Gallet, J.-C., Barret, M., Houdier, S., Voisin, D., Douglas, T. A., Blum, J. D., Beine, H. J., Anastasio, C., and Bréon, F.-M.: The specific surface area and chemical composition of diamond dust near Barrow, Alaska, *J. Geophys. Res.*, 116, D00R06, doi:10.1029/2011JD016162, 2011.
- France, J. L., King, M. D., Frey, M. M., Erbland, J., Picard, G., Preunkert, S., MacArthur, A., and Savarino, J.: Snow optical properties at Dome C (Concordia), Antarctica; implications for snow emissions and snow chemistry of reactive nitrogen, *Atmos. Chem. Phys.*, 11, 9787–9801, doi:10.5194/acp-11-9787-2011, 2011.
- Frey, M. M., Steward, R. W., McConnell, J. R., and Bales, R. C.: Atmospheric hydroperoxides in West Antarctica: links to stratospheric ozone atmospheric oxidation capacity, *J. Geophys. Res.*, 110, D23301, doi:10.1029/2005JD006110, 2005.
- Frey, M. M., Brough, N., France, J. L., Anderson, P. S., Traulle, O., King, M. D., Jones, A. E., Wolff, E. W., and Savarino, J.: The diurnal variability of atmospheric nitrogen oxides (NO and NO_2) above the Antarctic Plateau driven by atmospheric stability and snow emissions, *Atmos. Chem. Phys.*, 13, 304–3062, doi:10.5194/acp-13-3045-2013, 2013.
- Frey, M. M., Brough, N., Roscoe, H., Kukui, S., Savarino, J., Legrand, M., and Preunkert, S.: Drivers of atmospheric nitrogen oxide emissions from snow above the Antarctic Plateau

32057

- in summer: sensitivity to stratospheric ozone and impact on ozone production, submitted, 2014.
- Gallée, H. and Gorodetskaya, I.: Validation of a limited area model over Dome C, Antarctic 29 Plateau, during winter, 34, 61–72, *Clim. Dynam.*, doi:10.1007/s00382-008-0499-y, 2008.
- Gallée, H., Preunkert, S., Argentini, S., Frey, M. M., Genthon, C., Jourdain, B., Pietroni, I., Casasanta, G., Barral, H., Vignon, E., and Legrand, M.: Characterization of the boundary layer at Dome C (East Antarctica) during the OPALE summer campaign, *Atmos. Chem. Phys.*, in press, 2014.
- Helmig, D., Bocqueta, F., Cohena, L., and Oltmans, S. J.: Ozone uptake to the polar snowpack at Summit, Greenland, *Atmos. Environ.*, 41, 5061–5076, doi:10.1016/j.atmosenv.2006.06.064, 2007.
- Hutterli, M. A., Rothlisberger, R., and Bales, R. C.: Atmosphere-to-snow-to-firn transfer studies of HCHO at Summit, Greenland, *Geophys. Res. Lett.*, 26, 1691–1694, doi:10.1029/1999GL900327, 1999.
- Hutterli, M. A., Bales, R. C., McConnell, J. R., and Stewart, R. W.: HCHO in Antarctic snow: preservation in ice cores and air–snow exchange, *Geophys. Res. Lett.*, 29, 1235, doi:10.1029/2001GL014256, 2002.
- Hutterli, M. A., McConnell, J. R., Chen, G., Bales, R. C., Davis, D. D., and Lenschow, D. H.: Formaldehyde and hydrogen peroxide in air, snow and interstitial air at South Pole, *Atmos. Environ.*, 38, 5439–5450, 2004.
- Jun, L., Weili, W., and Zwally, H. J.: Interannual variations of shallow firn temperature at Greenland summit, *Ann. Glaciol.*, 35, 368–370, doi:10.3189/172756402781816933, 2002.
- Kukui, A., Legrand, M., Ancellet, G., Gros, V., Bekki, S., Sarda-Estève, R., Loisil, R., and Preunkert, S.: Measurements of OH and RO_2 radicals at the coastal Antarctic site of Dumont d’Urville (East Antarctica) in summer, *J. Geophys. Res.*, 117, D12310, doi:10.1029/2012JD017614, 2012.
- Kukui, A., Legrand, M., Preunkert, S., Frey, M. M., Loisil, R., Gil Roca, J., Jourdain, B., King, M. D., France, J. L., and Ancellet, G.: Measurements of OH and RO_2 radicals at Dome C, East Antarctica, *Atmos. Chem. Phys.*, 14, 12373–12392, doi:10.5194/acp-14-12373-2014, 2014.
- Legrand, M., Preunkert, S., Schock, M., Cerqueira, M., Kasper-Giebl, A., Afonso, J., Pio, C., Gelencsér, A., and Dombrowski-Etchevers.: Major 20th century changes of carbonaceous aerosol components (EC, WinOC, DOC, HULIS, carboxylic acids, and cellulose) derived from Alpine ice cores, *J. Geophys. Res.*, 112, D23S11, doi:10.1029/2006JD008080, 2007.

32058

- Legrand, M., Preunkert, S., Jourdain, B., Guilhermet, J., Fain, X., Alekhina, I., and Petit, J. R.: Water-soluble organic carbon in snow and ice deposited at Alpine, Greenland, and Antarctic sites: a critical review of available data and their atmospheric relevance, *Clim. Past*, 9, 2195–2211, doi:10.5194/cp-9-2195-2013, 2013.
- 5 Legrand, M., Preunkert, S., Frey, M., Bartels-Rausch, Th., Kukui, A., King, M. D., Savarino, J., Kerbrat, M., and Jourdain, B.: Large mixing ratios of atmospheric nitrous acid (HONO) at Concordia (East Antarctic Plateau) in summer: a strong source from surface snow?, *Atmos. Chem. Phys.*, 14, 9963–9976, doi:10.5194/acp-14-9963-2014, 2014.
- Lenschow, D. H.: Micrometeorological techniques for measuring biosphere–atmosphere trace gas exchange, in: *Biogenic Trace Gases: measuring emissions from soil and water*, edited by: Matson, P. A. and Harriss, R. C., Blackwell Science, London, 126–163, 1995.
- 10 Michalowski, B. A., Francisco, J. S., Li, S.-M., Barrie, L. A., Bottenheim, J. W., and Shepson, P. B.: A computer model study of multiphase chemistry in the Arctic boundary layer during polar sunrise, *J. Geophys. Res.*, 105, 15131–15145, , 2000.
- 15 Preunkert, S., Jourdain, B., Legrand, M., Udisti, R., Becagli, S., and Cerri, O.: Seasonality of sulfur species (sulfate, methanesulfonate and dimethyl sulfur) in Antarctica: inland versus coastal regions, *J. Geophys. Res.*, 113, D15302, doi:10.1029/2008JD009937, 2008.
- Preunkert, S., Ancellet, G., Legrand, M., Kukui, A., Kerbrat, M., Sarda-Estève, R., Gros, V., and Jourdain, B.: Oxidant Production over Antarctic Land and its Export (OPALE) project: an overview of the 2010–2011 summer campaign, *J. Geophys. Res.*, doi:10.1029/2011JD017145, 2012.
- 20 Preunkert, S., Legrand, M., Pépy, G., Gallée, H., Jones, A., and Jourdain, B.: The atmospheric HCHO budget at Dumont d'Urville (East Antarctica): contribution of photochemical gas-phase production versus snow emissions, *J. Geophys. Res. Atmos.*, 118, 13319–13337, doi:10.1002/2013JD019864, 2013.
- 25 Seok, B., Helmig, D., Williams, M. W., Liptzin, D., Chowanski, K., and Hueber, J.: An automated system for continuous measurements of trace gas fluxes through snow: an evaluation of the gas diffusion method at a subalpine forest site, Niwot Ridge, Colorado, *Biogeochemistry*, 95–95, 113, doi:10.1007/s10533-009-9302-3, 2009.

32059

Table 1. Gas-phase reactions included in the 1-D model (see Sect. 2.4). Kinetic rates are given in $\text{cm}^3 \text{molecule}^{-1} \text{s}^{-1}$. HCHO and MHP (CH_3OOH) photolysis rates are reported in Fig. 8.

No.	Reactions	Kinetic rates	References
R1	$\text{CH}_4 + \text{OH} + \text{O}_2 \rightarrow \text{CH}_3\text{O}_2 + \text{H}_2\text{O}$	$2.45 \times 10^{-12} \exp[-1775/T]$	a
R2	$\text{CH}_3\text{O}_2 + \text{NO} \rightarrow \text{CH}_3\text{O} + \text{NO}_2$	$2.30 \times 10^{-12} \exp[360/T]$	b
R3	$\text{CH}_3\text{O} + \text{O}_2 \rightarrow \text{HCHO} + \text{HO}_2$	$7.20 \times 10^{-14} \exp[-1080/T]$	b
R4	$\text{CH}_3\text{O}_2 + \text{CH}_3\text{O}_2 \rightarrow 2\text{CH}_3\text{O} + \text{O}_2$	$(7.40 \times 10^{-13} \exp[-520/T] - 1.03 \times 10^{-13} \exp[800/T])0.35$	b
R5	$\text{CH}_3\text{O}_2 + \text{CH}_3\text{O}_2 \rightarrow \text{CH}_3\text{OH} + \text{HCHO} + \text{O}_2$	$(1.03 \times 10^{-13} \exp[800/T])0.65$	b
R6	$\text{CH}_3\text{O}_2 + \text{HO}_2 \rightarrow \text{CH}_3\text{OOH} + \text{O}_2$	$3.80 \times 10^{-13} \exp[780/T]$	b
R7	$\text{CH}_3\text{OOH} + \text{OH} \rightarrow \text{HCHO} + \text{HO} + \text{H}_2\text{O}$	$(2.93 \times 10^{-12} \exp[190/T])0.35$	b
R8	$\text{CH}_3\text{OOH} + \text{OH} \rightarrow \text{CH}_3\text{O}_2 + \text{H}_2\text{O}$	$(1.78 \times 10^{-12} \exp[220/T])0.65$	b
R9	$\text{HCHO} + \text{OH} \rightarrow \text{H}_2\text{O} + \text{HCO}$	$5.40 \times 10^{-12} \exp[135/T]$	b
R10	$\text{CH}_3\text{OOH} \rightarrow \text{CH}_3\text{O} + \text{OH}$ ($\lambda < 645 \text{ nm}$)	J_{MHP}	
R11	$\text{HCHO} \rightarrow \text{H}_2 + \text{CO}$ ($\lambda < 337 \text{ nm}$)	$J_{\text{HCHO-mol}}$	
R12	$\text{HCHO} \rightarrow \text{H} + \text{HCO}$ ($\lambda < 360 \text{ nm}$)	$J_{\text{HCHO-rad}}$	
R13	$\text{Br} + \text{HCHO} \rightarrow \text{HBr} + \text{HCO}$	$2.7 \times 10^{-12} \exp[-580/T]$	c
R14	$\text{BrO} + \text{CH}_3\text{O}_2 \rightarrow \text{CH}_2\text{O}_2 + \text{HOBr}$	5.70×10^{-12}	d
R15	$\text{BrO} + \text{HCHO} \rightarrow \text{HOBr} + \text{HCO}$	1.50×10^{-14}	e

^a DeMore et al. (1997), ^b Atkinson et al. (2006), ^c Atkinson et al. (2007), ^d Atkinson et al. (2008), ^e Michalowski et al. (2000).

32060

Table 2. Atmospheric HCHO mixing ratios in the lower Antarctic atmosphere.

Site	Date	HCHO (pptv)	Location	References
South Pole	Dec 2000	103	89.98° S 24.8° W	Hutterli et al. (2004)
South Pole	2–4 Jan 2003	155	89.91° S 147.57° W	Frey et al. (2005)
Byrd	28 Nov 2011–11 Dec 2002	120 ± 50	80.02° S 119.6° W	Frey et al. (2005)
Halley	Dec 2004–Jan 2005	90–140	75.58° S 26.65° W	Salmon et al. (2008)
DDU	Jan 2009 and Dec 2009	150–195	66.66° S 140.02E	Preunkert et al. (2013)
Concordia	14 Dec 2011–11 Jan 2012	129 ± 37	75.1° S 123.55° E	This study

32061

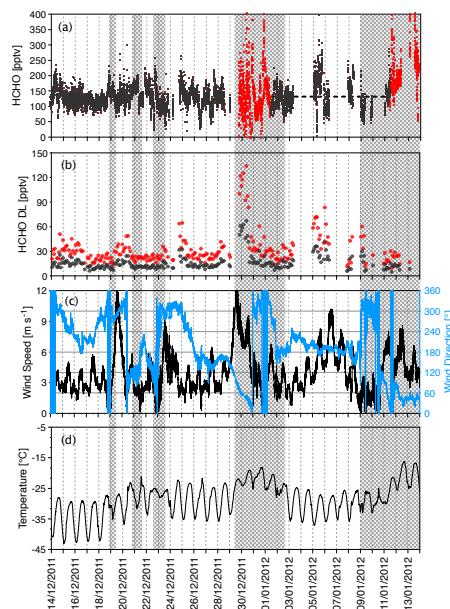


Figure 1. (a) HCHO mixing ratios (time interval of 30 s) measured during the 2011/12 OPAL campaign at 1 m above the snow surface, red points refer to periods during which contamination by wind transport from the station is suspected. The horizontal dashed line indicates the mean mixing ratio observed between 1 and 11 January, a period over which the sampling was very discontinuous. (b) Detection limits (DL), taken as one and two SDs of raw zero values measured every two hours. (c) Wind speed and direction. (d) Air temperature. Grey bands denote periods during which clouded sky conditions prevailed.

32062

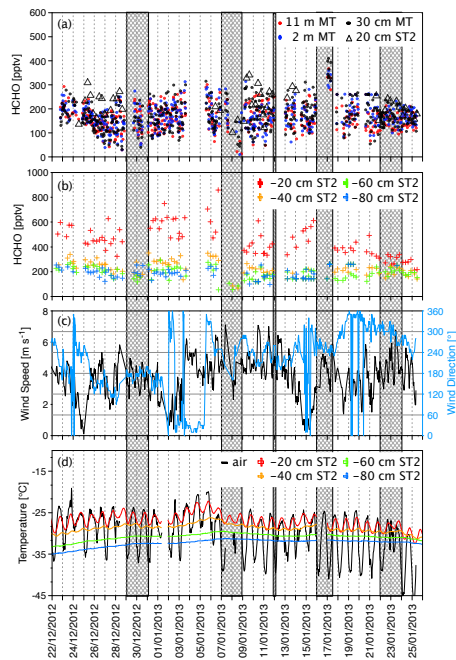


Figure 2. (a) 10 min averaged HCHO mixing ratios observed in the ambient air during the 2012/13 campaign at 3 different heights above the snow on the Meteorological Tower (MT) and at 20 cm on the Snow Tower 2 (ST2) (see Sect. 2.3). (b) 10 min averaged HCHO measured at different depths in the snowpack on ST2. (c) Wind speed and direction. (d) Temperature of air and in snow at different depths (ST2). Grey bands denote periods for which data were not considered due to technical problems of the analyzer and/or the snow tower system. They separate the 6 time intervals over which data were averaged.

32063

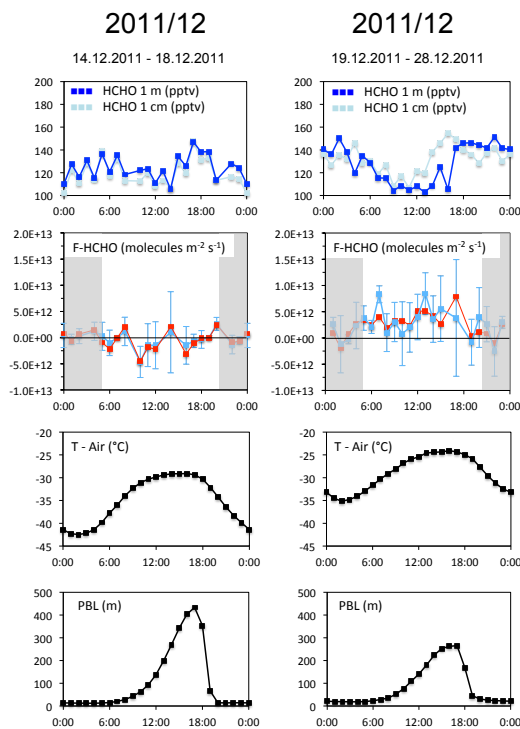


Figure 3. From top to bottom: mean daily course (hours are in LT) of HCHO mixing ratios measured at 1 m and 1 cm above the ground, snow to air fluxes calculated from observed vertical gradients between 1 m and 1 cm (arithmetic means in blue, median values in red), measured ambient air temperatures at Concordia, and simulated PBL heights.

32064

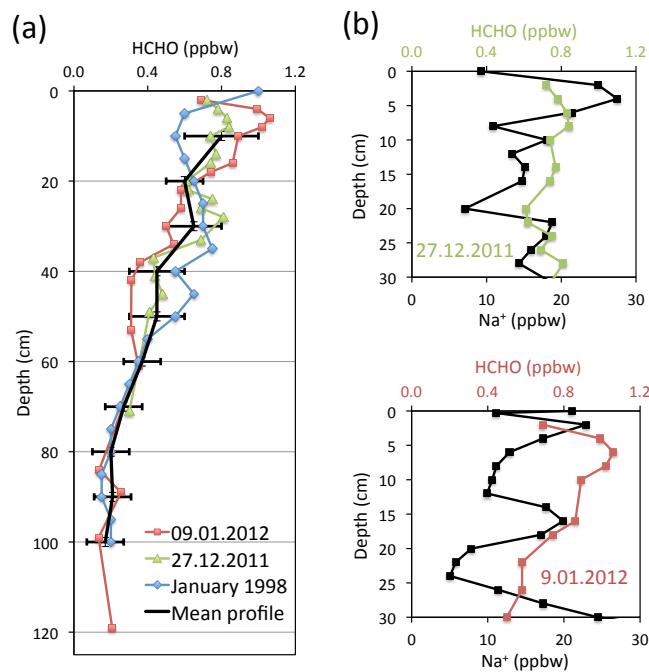


Figure 4. (a) Vertical profiles of HCHO in bulk snow at Concordia. The vertical snow profiles of HCHO obtained from the two snow-pits dug during the 2011/12 campaign are compared to the one from Hutterli et al. (2002). (b) Sodium vs. HCHO content in the upper 30 cm of the two snow-pits dug in 2011/12.

32065

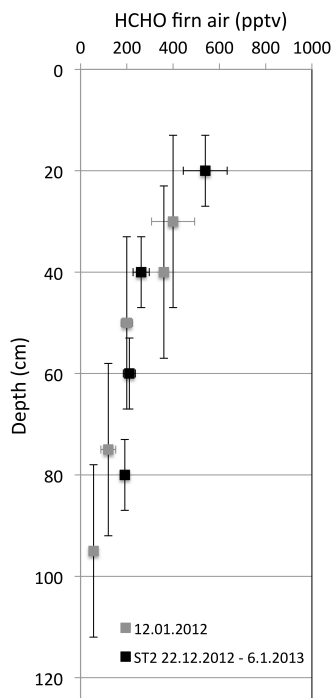


Figure 5. Vertical profiles of HCHO in interstitial air at Concordia. Vertical bars refer to the depth from which 66 % of air was sampled (see Sect. 2.3) and the horizontal ones to SDs of 10 min and 30 s means for 2012/13 and 2011/12, respectively.

32066

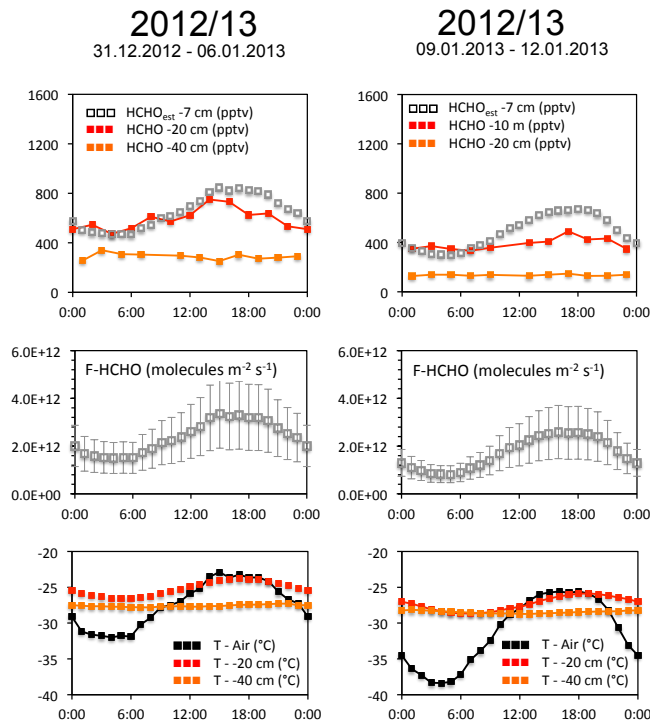


Figure 6. Top: mean daily course (hours are in LT) of firn air HCHO mixing ratios at different depths. At 7 cm below the snow surface, HCHO mixing ratios were estimated. Second from top: HCHO flux calculated from firn air atmosphere gradients. Error bars refer to uncertainties in depth (± 3 cm) and in snow concentration (± 0.08 ppbw) (see text in Sect. 3.3). Bottom air and firn air temperatures.

32067

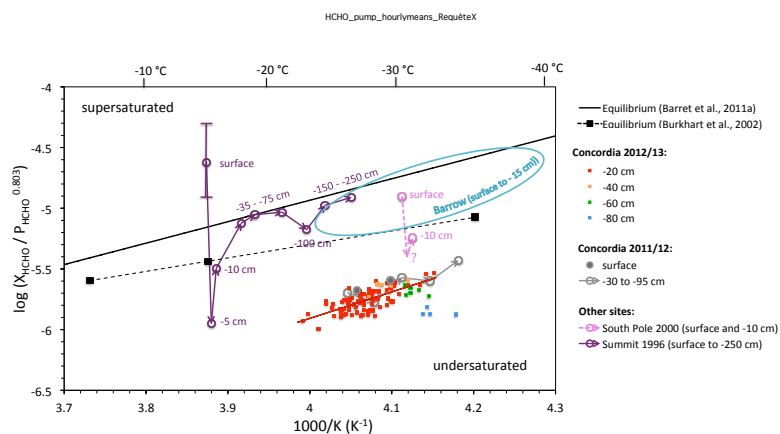


Figure 7. Arrhenius plot of the partitioning coefficient $K(T)$ for HCHO in firn air and snow of Concordia, South Pole, Summit and Barrow vs. T^{-1} . The thermodynamic equilibrium as estimated by Barret et al. (2011a) is reported as black line. Barrow data, which use however ambient air and not firn air measurements, are situated in the blue ellipse (Barret et al., 2011b). See discussion in text. Summit snow temperatures were calculated after (Jun et al., 2002).

32068

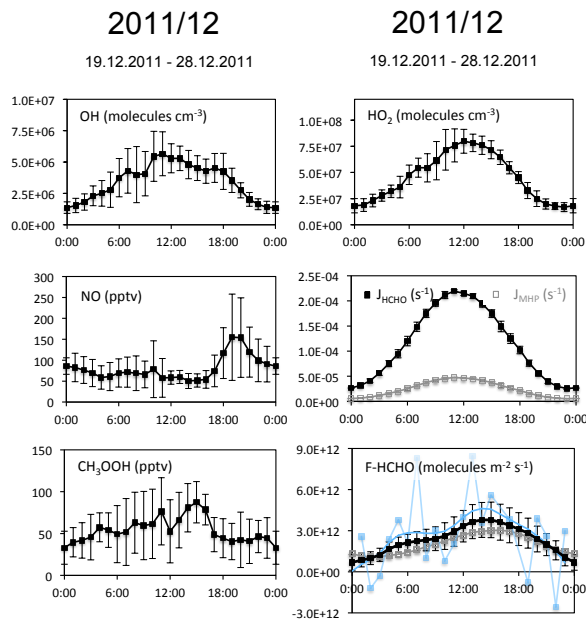


Figure 8. Diurnal cycles (hours are in LT) of key input parameters used in 1-D simulations discussed in Sect. 6. J_{HCHO} denotes the sum of $J_{\text{HCHO-mol}}$ and $J_{\text{HCHO-rad}}$ (see Table 1). HCHO fluxes (F-HCHO) used in the model were taken as the mean (black dots) of F-HCHO derived from atmospheric HCHO gradients (blue dots) and from those derived from firn air atmosphere gradients (grey dots). Vertical bars refer to daily variability and to the uncertainty of calculations in the case of F-HCHO, respectively. OH and HO₂ data are from Kukui et al. (this issue), NO from Frey et al. (2014).

32069

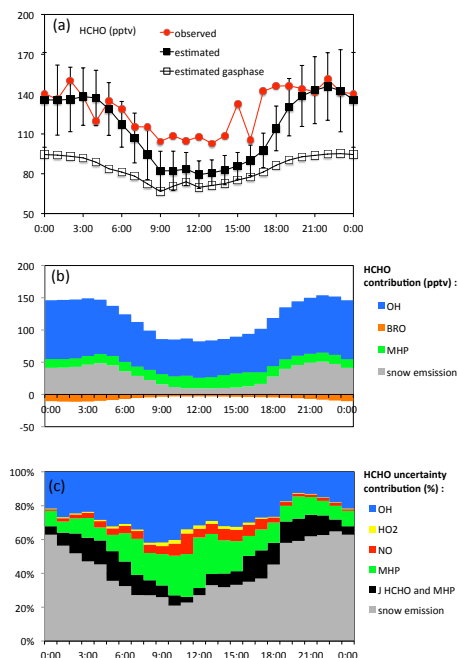


Figure 9. Diurnal cycles (hours are in LT) of: **(a)** HCHO simulated (squares) and observed (red circles) mixing ratios, grey open squares refer to values simulated when only the gas phase chemistry is considered whereas solid black squares refer to values simulated when both gas-phase chemistry and snow emissions are considered (see Sect. 6). The vertical bars reported on simulated values correspond to uncertainties related to the daily variability and calculation uncertainties of parameters reported in Fig. 8. **(b)** Simulated HCHO contributions of the different gas-phase mechanisms. **(c)** Contribution of the different uncertainties making up the vertical error bars in **(a)**.

32070